Trial-Aligned Joint EEG–Behaviour Modelling for Pedestrian Road-Crossing Decisions: Cross-Modal Prediction Beyond Two-Stage Pipelines.

Jamal Amani Rad, Thomas O. Hancock, Stephane Hess, and Gustav Markkula

Institute for Transport Studies, University of Leeds, Leeds, UK

Short summary

Pedestrian road-crossing is a safety-critical, time-pressured decision that produces both choices and response times, and recent work has analysed EEG correlates such as the centro-parietal positivity (CPP) in a separate, post-hoc step. We present a single-trial joint neurocognitive model that treats crossing choice, response time, and trial-wise CPP features as co-generated by shared latent evidence-accumulation dynamics. The model is fitted hierarchically to an EEG+behaviour pedestrian crossing dataset with repeated time-to-arrival manipulations, using simulation-based Bayesian inference. The joint formulation enables cross-modal prediction (early EEG windows sharpening predictions of imminent choice/RT; observed behaviour predicting CPP) and provides an explicit trial-alignment diagnostic via EEG–behaviour shuffling. Results show that one parameterisation can reproduce behavioural and neural patterns simultaneously and yields improved mechanistic interpretability compared to two-stage pipelines, supporting more robust prediction and model checking in road-user behaviour research.
Keywords: EEG; Evidence accumulation; Pedestrian road crossing; Response time; Simulation-based inference; Single-trial joint modelling.

1 Introduction

Pedestrian road-crossing is a safety-critical decision in which people must commit to an action under time pressure, trading off mobility benefits against collision risk while perceptual evidence evolves continuously as an oncoming vehicle approaches. For transport systems—and especially for automated vehicles that must anticipate and negotiate with vulnerable road users—the modelling challenge is therefore not only to predict *whether* a pedestrian will cross, but also *when* they will do so, and how this timing reflects underlying decision processes (Camara et al., 2021; Markkula et al., 2020). Evidence-accumulation models (EAMs), and in particular drift–diffusion formulations, provide a principled account of joint choice and response time (RT) by linking behaviour to latent decision dynamics with interpretable parameters (Ratcliff, 1978; Ratcliff and McKoon, 2008; Bogacz et al., 2006). In the road-crossing context, recent work has operationalised these dynamics using alternative theoretical accounts of the evidence driving accumulation, including perception-based heuristics and utility-based formulations grounded in risk–reward trade-offs (Pekkanen et al., 2022; Lin et al., 2022; Markkula et al., 2023; Ma et al., 2025).

In parallel, cognitive neuroscience has established robust neural signatures of evidence accumulation. Most prominently, the centro-parietal positivity (CPP) exhibits a characteristic build-up and peaks around response execution, and is widely interpreted as an accumulation-to-bound signal (O'Connell et al., 2012; Kelly and O'Connell, 2013). Single-trial CPP measures have been related to trial-wise decision variables and diffusion-model parameters in laboratory tasks (Nunez et al., 2017; van Vugt et al., 2019; Yau et al., 2021), motivating recent efforts to incorporate EEG into applied decision modelling. Notably, Ma et al. (2025) demonstrated a clear CPP signature in a controlled pedestrian road-crossing paradigm and used CPP correlations with model-derived accumulated evidence to arbitrate between competing drift–diffusion accounts of crossing behaviour.

Despite this convergence, the dominant workflow in applied road-user decision research remains effectively two-stage: behavioural data are first fitted with an EAM (or other choice/RT model), EEG features are then extracted and analysed separately, and the two are finally linked using post-hoc correlations or regressions (Purcell et al., 2010; Turner et al., 2015; Ma et al., 2025). This separation is more than a matter of convenience. It implicitly relaxes the core scientific claim motivating the use of EEG—namely that neural signals and behaviour are expressions of a

shared, *trial-wise* generative decision process. As a result, two-stage analyses cannot (i) provide *cross-modal* predictions (e.g., forecasting imminent crossing decisions and RTs from early EEG windows, or predicting trial-wise CPP conditional on behavioural outcomes), (ii) quantify trial-level brain–behaviour coupling under a single likelihood where both modalities constrain the same latent variables, or (iii) adjudicate mechanistic alternatives in a unified inferential framework rather than via separate behavioural fit plus neural plausibility checks (Turner et al., 2013; Palestro et al., 2018; Ghaderi-Kanghavari et al., 2023). In short, linking EEG and behaviour "after the fact" forfeits exactly the trial-level coupling that makes neurocognitive modelling informative for mechanism and prediction.

In this paper we address this gap by introducing and demonstrating a *trial-aligned* joint EEG–behaviour modelling approach for pedestrian road-crossing decisions. Building on integrative neurocognitive modelling frameworks developed in mathematical psychology (Turner et al., 2013; Palestro et al., 2018; Ghaderi-Kanghavari et al., 2023), we formulate a single generative model in which crossing choice, RT, and trial-wise CPP summaries are co-generated from shared latent evidence-accumulation dynamics, estimated hierarchically at the participant level. Because closed-form likelihoods for the full multimodal model are generally unavailable, we adopt simulation-based Bayesian inference with amortisation (Radev et al., 2023), enabling scalable posterior inference for both cognitive parameters and brain–behaviour coupling parameters. Using the pedestrian road-crossing dataset of Ma et al. (2025), with repeated manipulation of time-to-arrival (TTA) and simultaneous EEG recording, we evaluate the joint model with posterior predictive checks in both modalities and demonstrate two distinctive capabilities that are not accessible in a two-stage pipeline: (i) cross-modal prediction (EEG→behaviour and behaviour→EEG) with Bayesian uncertainty quantification, and (ii) an explicit diagnostic of trial-level coupling via EEG–behaviour trial shuffling (Ghaderi-Kanghavari et al., 2023). The contribution is therefore not merely to "add EEG" to an existing behavioural model, but to provide a coherent inferential framework in which neural and behavioural data jointly constrain the same decision process, enabling stronger mechanistic commitment and more actionable prediction for road-user behaviour modelling.

2 Methodology

Dataset and experimental task. We analyse a controlled pedestrian road-crossing dataset with simultaneously recorded behaviour and EEG (full details of the experiment are provided in Ma et al. 2025). Sixteen right-handed participants (9 male; age range 26–42 years) completed a computer-based crossing task in a simulated road environment (see Figure 1). Each trial began with an auditory cue and a fixation cross presented on a grey background for a randomly jittered interval (2.0 s, 2.5 s, or 3.0 s). A vehicle stimulus then appeared centrally on the screen, marking stimulus onset ($t = 0$) and the start of an approach phase in which a car moved toward the participant's crossing point. The initial vehicle distance was fixed at 40 m and the vehicle approached at one of four TTA conditions: 2.5 s, 3.0 s, 3.5 s, and 4.0 s, implemented via corresponding speeds (16.0, 13.33, 11.42, and 10.0 m/s) with a small per-trial temporal jitter (±0.1 s) to reduce discrete-condition recognisability. Approach direction (left vs. right) was counterbalanced, and no auditory cues accompanied vehicle motion to avoid multimodal timing cues. Participants initiated a crossing at a self-chosen time by keypress, after which the viewpoint translated across a 4.2 m road at a fixed walking speed of 1.6 m/s; collisions triggered an auditory warning at collision time. Each participant completed a 16-trial practice block followed by four experimental blocks of 64 trials each (4 TTA × 2 directions × 8 repetitions), yielding 256 trials per participant with fully randomised order within blocks.

Each trial provides: (i) a binary decision outcome, coded as crossing *before* versus *after* the vehicle passed the crossing point (cross-before vs. cross-after), and (ii) a response time, defined as the time from vehicle onset to the crossing keypress. We focus on modelling the full distribution of RT jointly with decision outcome, rather than conditioning on decisions, because the key scientific quantity of interest is the latent decision dynamics that simultaneously determine *which* action is selected and *when* it is executed.

EEG acquisition, preprocessing, and CPP feature construction for joint modelling. EEG was recorded using a Biosemi ActiveTwo system with a 64-channel 10–20 montage (plus EOG and mastoids) at 1024 Hz and subsequently downsampled to 256 Hz. Our objective is not a condition-level ERP contrast, but a *trial-level* neural measurement suitable for a generative joint model. Accordingly, preprocessing is designed to (a) preserve the slow centro-parietal components relevant to CPP while (b) removing ocular/muscle artefacts robustly at the single-trial level.

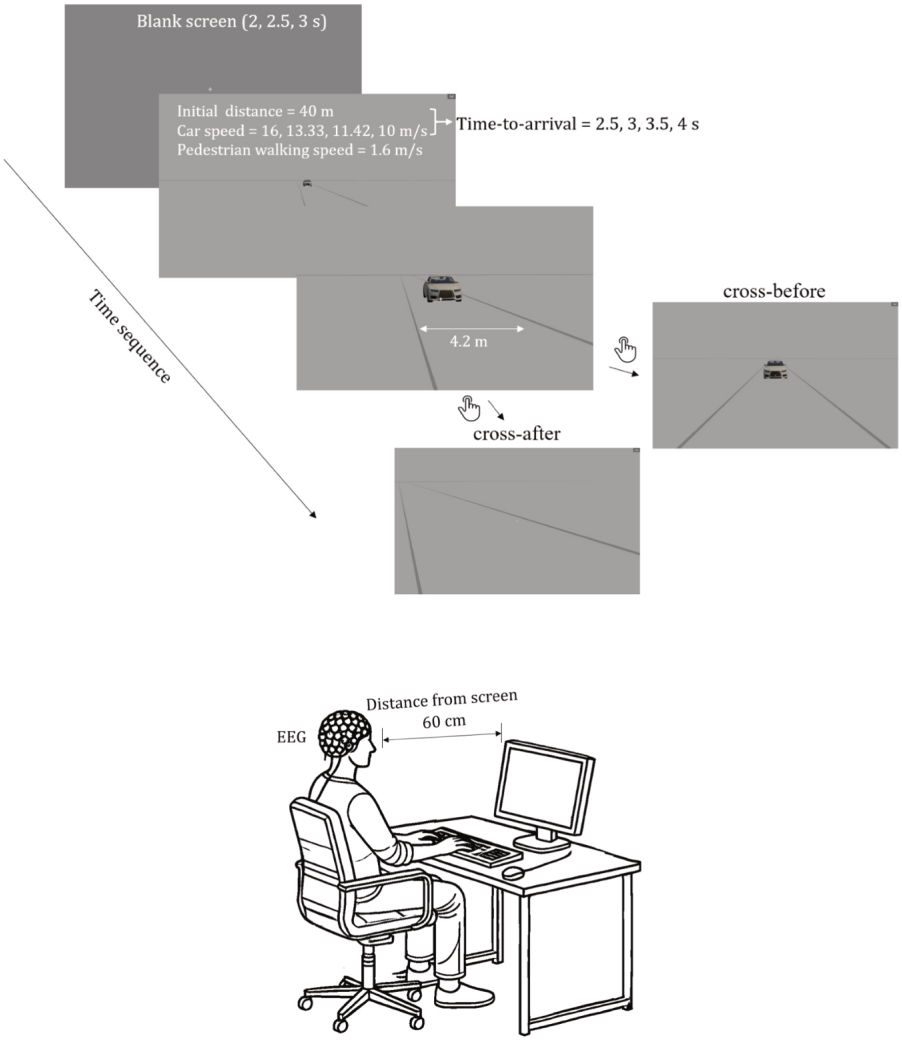


Figure 1: Example of one trial of the pedestrian crossing experiment, and schematic of the task setup. Adapted from Ma et al. (2025).

Concretely, continuous EEG is first inspected for gross channel failures and re-referenced to the average reference. We apply a conservative low-pass filter (40 Hz) to attenuate high-frequency noise while keeping ERP morphology intact. To mitigate the known sensitivity of independent component analysis (ICA) to very low high-pass cut-offs, we estimate ICA decomposition on a moderately high-pass-filtered copy of the data (e.g., 1 Hz), identify artefact components using EOG channels and component topographies/time courses, and then apply the learned unmixing to a minimally high-pass-filtered copy (e.g., 0.1 Hz) used for CPP estimation; this preserves slow CPP-related activity while benefiting from stable ICA estimation. Data are then epoched around (i) stimulus onset (stimulus-locked) and (ii) the behavioural response (response-locked). A baseline correction is applied using a short pre-stimulus interval (e.g., $[-200, 0]$ ms relative to car onset). Epoch-level artefact rejection is performed using automated statistical thresholding (e.g., FASTER) followed by visual spot checks to ensure that remaining epochs are suitable for single-trial modelling.
We then derive a CPP time series as an average over a centro-parietal cluster centred on Pz (e.g., CPz, Pz, POz, P1, P2), consistent with the CPP literature (O'Connell et al., 2012; Kelly and O'Connell, 2013). For each trial we construct a compact CPP feature used in the joint likelihood. In the main analyses we use a response-locked pre-response summary,

$$CPP_{ij} = \frac{1}{|\mathcal{W}|} \int_{t \in \mathcal{W}} \widetilde{y}_{ij}(t)\, dt, \tag{1}$$

where $\widetilde{y}_{ij}(t)$ is the response-locked CPP trace for participant i and trial j, and $\mathcal{W}$ is a fixed pre-response window (e.g., $[-400, 0]$ ms). This window targets the build-up phase most diagnostic of accumulation dynamics (O'Connell et al., 2012; Kelly and O'Connell, 2013). (In robustness

checks, we also consider slope-based summaries over the same window, obtained by least-squares regression of $\widetilde{y}_{ij}(t)$ on time; the joint model below accommodates either choice by redefining CPP_{ij} accordingly.)

Behavioural decision dynamics: a time-varying evidence-accumulation core. Let $x_{ij}(t)$ denote a latent decision variable that evolves from stimulus onset until a decision is reached. We model $x_{ij}(t)$ as a stochastic accumulation process,

$$dx_{ij}(t) \;=\; v_{ij}(t)\,dt \;+\; \sigma\,dW(t), \tag{2}$$

where $W(t)$ is a Wiener process and σ controls within-trial stochasticity. The decision outcome is determined by the first time τ_{ij} at which $x_{ij}(t)$ hits one of two absorbing bounds, corresponding to cross-before and cross-after. To capture time pressure inherent in road-crossing, we allow bounds to be time-varying (collapsing), implementing an urgency-like mechanism (Ratcliff and McKoon, 2008; Malhotra et al., 2018). A convenient parameterisation expresses the bound half-separation as a smooth function of remaining time-to-arrival, $TTA_{ij}(t) = TTA_{0,ij} - t$:

$$a_{ij}(t) \;=\; a_{0,i}\left[1+\exp\{-\kappa_i\,(TTA_{ij}(t)-\tau_i)\}\right]^{-1}, \tag{3}$$

so that the effective bound $\pm a_{ij}(t)$ decreases as the vehicle approaches (smaller remaining TTA), reflecting increased urgency to commit.

The drift term $v_{ij}(t)$ operationalises how approaching-vehicle dynamics shape instantaneous evidence. We use a utility-grounded specification that encodes the trade-off between mobility benefit and collision-related cost, consistent with utility-based formulations of road-user interaction (Lin et al., 2022; Markkula et al., 2023). Specifically, let U_i denote a per-participant baseline utility rate for making progress, and let the collision-cost rate increase as time-to-arrival decreases,

$$C_i(t) \;=\; \frac{k_i}{TTA_{ij}(t)} \quad \text{for } TTA_{ij}(t) > 0, \tag{4}$$

where $k_i > 0$ quantifies risk sensitivity. We define the drift as the discounted difference between the prospective value of crossing now versus waiting until after vehicle passage, implemented as

$$v_{ij}(t) \;=\; \eta_i \int_t^{TTA_{0,ij}} \tanh\big(U_i - C_i(t')\big)\,dt', \tag{5}$$

where $\eta_i > 0$ is a scaling parameter and $\tanh(\cdot)$ ensures bounded contributions as collision cost diverges near vehicle arrival. This specification yields positive drift favouring cross-before when the net prospective utility of crossing is high, and negative drift when collision cost dominates, while naturally producing stronger temporal nonlinearity at short TTA (where risk escalates rapidly).

Observed response time is the sum of decision time and non-decision time,

$$RT_{ij} \;=\; \tau_{ij} + t_i^{\mathrm{nd}}, \qquad t_i^{\mathrm{nd}} \sim \mathcal{N}^{+}(\mu_i^{\mathrm{nd}}, \sigma_i^{\mathrm{nd}}), \tag{6}$$

with $\mathcal{N}^{+}$ a truncated normal to enforce positivity (Ratcliff and McKoon, 2008).

Neural observation model: CPP as a noisy readout of latent accumulation. To link EEG and behaviour at the trial level, we treat CPP as an additional observation generated from the *same* latent accumulation process. The CPP feature in Eq. 1 is modelled as a noisy linear readout of a decision-relevant latent quantity. Let

$$z_{ij} \;=\; \frac{1}{|\mathcal{W}|}\int_{t\in\mathcal{W}} x_{ij}(t)\,dt \tag{7}$$

denote the latent evidence averaged over the same response-locked window used for CPP. We then specify

$$CPP_{ij} \;=\; \alpha_i + \lambda_i\, z_{ij} + \epsilon_{ij}, \qquad \epsilon_{ij} \sim \mathcal{N}(0, \sigma^2_{\mathrm{cpp},i}), \tag{8}$$

where α_i captures participant-specific baseline offsets and λ_i is a participant-specific brain–behaviour coupling strength. This simple but interpretable mapping operationalises the central mechanistic hypothesis that CPP indexes evidence accumulation (O'Connell et al., 2012; Kelly and O'Connell, 2013; Nunez et al., 2017). Importantly, Eq. 8 is defined at the *single-trial* level and shares latent drivers with the behavioural likelihood, enabling genuine cross-modal prediction. (In extensions, the same framework permits alternative commitments by redefining z_{ij}, e.g. using boundary proximity $x_{ij}(t)/a_{ij}(t)$ or an urgency term derived from $a_{ij}(t)$).

Hierarchical structure and priors. All key parameters vary across participants under a hierarchical model to capture heterogeneity while borrowing strength across the group (Turner et al., 2013; Palestro et al., 2018). For example, we place weakly informative priors on log-scale parameters to enforce positivity,

$$\begin{aligned} \log a_{0,i} &\sim \mathcal{N}(\mu_{a_0}, \sigma_{a_0}), & \log k_i &\sim \mathcal{N}(\mu_k, \sigma_k), \\ \log \eta_i &\sim \mathcal{N}(\mu_\eta, \sigma_\eta), & \lambda_i &\sim \mathcal{N}(\mu_\lambda, \sigma_\lambda), \end{aligned} \tag{9}$$

with hyperpriors on group-level means and scales chosen to be diffuse relative to plausible behavioural/EEG ranges. This yields posterior distributions at both participant and population levels for behavioural dynamics and neural coupling.

Inference, model checking, and trial-alignment diagnostic. The joint model defines a simulator that produces $(y_{ij}, RT_{ij}, CPP_{ij})$ from parameters via Eqs. 2–8. Because closed-form likelihoods for the full multimodal model are not generally available once neural observation and time-varying dynamics are combined, we use amortized simulation-based Bayesian inference (Radev et al., 2023). In brief, we simulate many datasets from the prior, train a neural posterior estimator to approximate $p(\theta \mid \mathcal{D})$, and then obtain fast posterior draws for the observed dataset without bespoke per-dataset MCMC.
Model adequacy is assessed through posterior predictive checks in *both* modalities: the posterior predictive distribution must reproduce (i) choice proportions and RT distributions across TTA conditions and (ii) CPP feature distributions and their condition-dependent shifts. Finally, because the model asserts genuine trial-wise coupling, we include a trial-alignment control: within each participant we randomly permute CPP features across trials while keeping behavioural data fixed, refit (or re-evaluate) the model, and quantify the degradation in posterior predictive performance. A pronounced degradation indicates that the model relies on within-trial alignment rather than only condition-level covariation, providing a direct diagnostic that is unavailable in two-stage correlation pipelines.

3 Results and discussion

Joint posterior predictive adequacy across modalities

Figure 2 provides distributional posterior predictive checks (PPCs) for behaviour (RT) and EEG (CPP feature), separately for cross-before and cross-after responses, and for each of the four TTA levels. Across all panels, the joint model reproduces not only central tendency but also the overall *shape* of the observed distributions, including the condition-dependent shifts in both RT and CPP. For cross-before trials, the RT mass is concentrated in the sub-second range, while for cross-after trials RTs shift to later times and broaden, with clear TTA-dependent movement of the distributions; the model tracks these systematic shifts closely (Fig. 2, top row). Critically, this fit is not confined to behaviour: the CPP feature distributions also shift with TTA for both response types, and the model captures these shifts without requiring a separate EEG-only stage (Fig. 2, bottom row). Taken together, these PPCs support the core claim of the approach: a single trial-wise generative parameterisation can account for *both* observed behaviour and EEG summaries simultaneously, rather than treating EEG as a post-hoc correlate.

Trial-wise brain–behaviour coupling via latent evidence

A central mechanistic commitment of the joint model is that single-trial neural variability should be partly explained by latent decision dynamics. Figure 3 visualises this coupling by relating the observed CPP feature to the trial-wise latent evidence summary z_{ij} (posterior mean). The positive association is substantial ($r = 0.51$), indicating that a meaningful proportion of CPP variability aligns with the latent decision variable rather than being purely measurement noise or condition-level averaging. This result is important for two reasons. First, it supports an *integrative* interpretation of CPP in this task: CPP fluctuations covary with the same trial-level decision quantity that drives choice and RT, consistent with an accumulation-to-bound account. Second, it clarifies why two-stage pipelines can be limiting: if CPP carries trial-wise information about z_{ij}, then collapsing EEG into condition contrasts and correlating afterwards discards precisely the alignment that the joint model exploits.

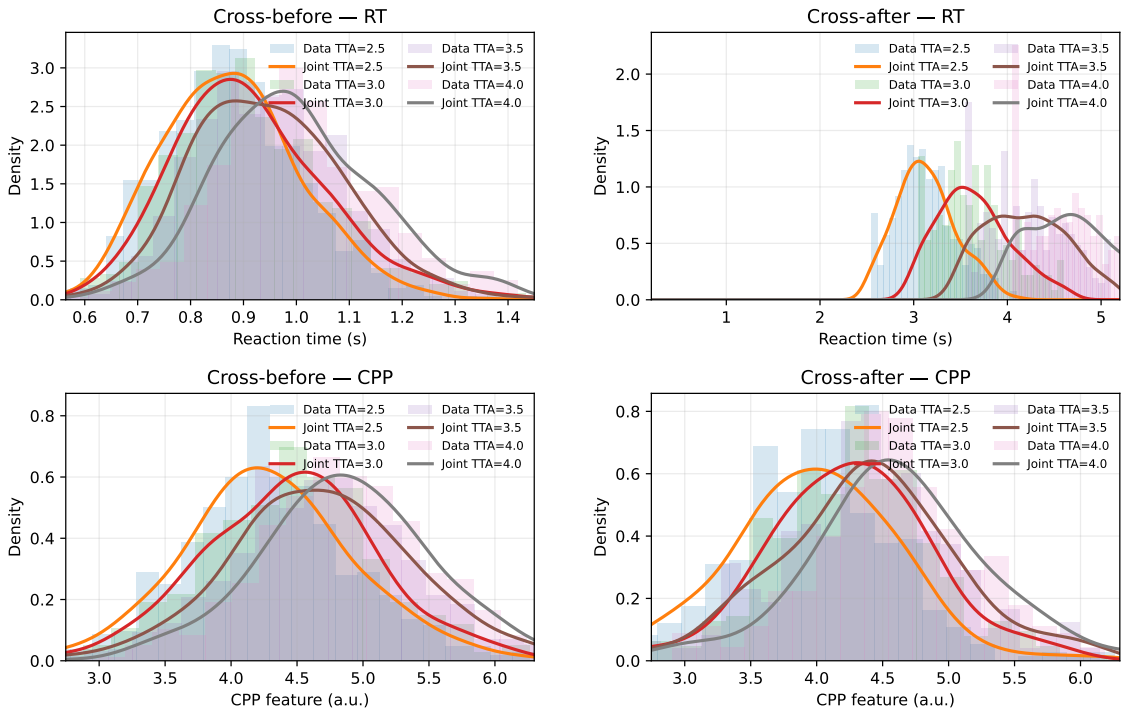


Figure 2: **Distributional PPCs for behaviour and EEG across TTA.** Observed (histograms) and joint-model predictive densities (lines) for RT and CPP features, shown separately for cross-before and cross-after responses across four TTA levels.

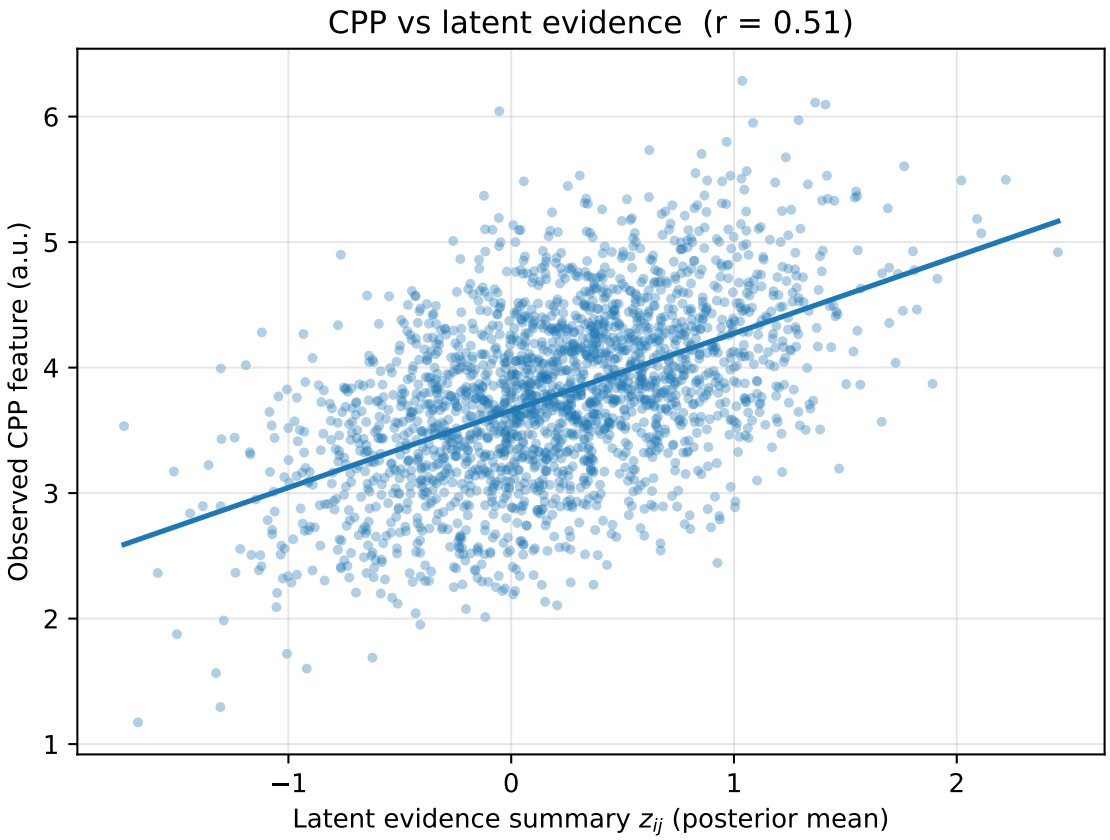


Figure 3: **Trial-wise coupling between latent evidence and CPP.** Scatter of observed CPP feature against the trial-wise latent evidence summary z_{ij} (posterior mean), with fitted regression line and correlation.

Cross-modal prediction and an explicit trial-alignment stress test

Figure 4 summarises what becomes possible once EEG and behaviour are fit jointly.

EEG → behaviour. The ROC analysis shows that including an early EEG feature in addition to TTA yields a large predictive gain for trial-wise crossing choice: the baseline model using TTA only achieves AUC = 0.66, whereas the aligned joint model achieves AUC = 0.92 (Fig. 4, top-left; see also the summary bars, bottom-left). This gap indicates that the EEG feature provides incremental, behaviour-relevant information beyond experimental condition (TTA). Crucially, the partially shuffled control reduces performance to AUC = 0.70, consistent with the idea that correct trial alignment is necessary to extract the strongest EEG-to-choice signal (Fig. 4, top-left). The fact that performance does not collapse all the way back to baseline under partial shuffling is also interpretable: shuffling that preserves some structure (e.g., within-condition distributions) can retain a residual condition-level association, but the marked drop from 0.92 to 0.70 indicates that the model's best predictive performance relies on within-trial coupling.

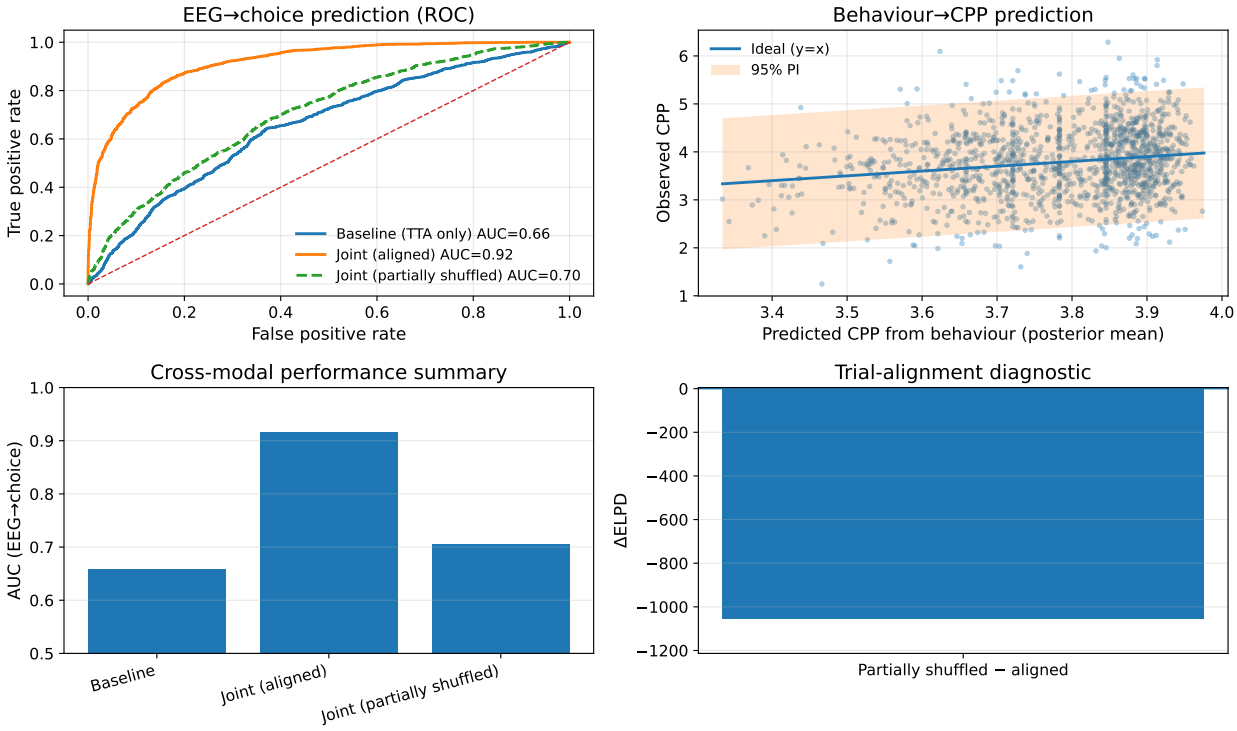


Figure 4: **Cross-modal prediction and trial-alignment diagnostics.** Top-left: EEG→choice ROC curves comparing a TTA-only baseline against the aligned joint model and a partially shuffled control. Top-right: Behaviour→CPP predictive check with 95% predictive interval. Bottom-left: AUC summary. Bottom-right: trial-alignment penalty expressed as ΔELPD (partially shuffled minus aligned).

Behaviour → EEG. The reverse direction is assessed via the predictive check relating the model's CPP predictions from behavioural variables to observed CPP (Fig. 4, top-right). The scatter is noisy—as expected for single-trial EEG—but the model's predictive interval provides a calibrated envelope capturing the dominant trend and the dispersion of observations. This is practically useful: it turns the EEG component into an explicit probabilistic prediction target rather than a qualitative plausibility check.

Alignment diagnostic in the likelihood domain. Finally, the trial-alignment diagnostic quantifies the cost of breaking trial-wise pairing in the model's predictive accuracy, here summarised as a large negative ΔELPD for "partially shuffled minus aligned" (Fig. 4, bottom-right). This provides a model-based stress test that directly targets the core modelling assumption: if EEG and behaviour are coupled at the trial level, then disrupting alignment must reduce joint predictive performance.

Overall, the results support three headline conclusions. (1) The joint model achieves strong distributional adequacy for both behaviour and EEG across conditions, demonstrating that the integration is not achieved by sacrificing behavioural fit. (2) The latent decision variable explains a substantial component of single-trial CPP variability ($r = 0.51$), offering a mechanistic link between accumulation dynamics and EEG on the same trials. (3) Joint inference enables genuinely cross-modal predictions (EEG $\leftrightarrow$ behaviour) and allows trial alignment to be tested explicitly via both discrimination (AUC) and likelihood-based criteria (ΔELPD), which are not naturally available in two-stage pipelines.

4 Conclusion

We introduced and validated a single-trial *joint* neurocognitive choice modelling approach that replaces two-stage EEG–behaviour pipelines with one coherent generative account of choice, reaction time, and EEG. The joint model achieved strong posterior predictive adequacy across modalities and conditions, and provided an explicit mechanistic link between trial-wise latent decision dynamics and CPP. Importantly, the framework enabled genuinely cross-modal inference—predicting behaviour from early EEG and predicting EEG from behaviour—with performance that depended on correct trial alignment, offering a direct diagnostic of trial-level coupling that is unavailable in standard workflows. These results support the feasibility and value of importing integrative neurocognitive modelling into applied choice modelling, and motivate the next steps of extending the same joint framework to additional datasets, alternative neural commitments (e.g., drift vs urgency vs boundary coupling), and richer task manipulations to sharpen mechanistic conclusions and broaden predictive utility.

Acknowledgements

Jamal Amani Rad, Stephane Hess and Thomas Hancock acknowledge the financial support by the European Research Council through the advanced grant 101020940-SYNERGY. Thomas Hancock's time was partially supported by Charisma Choudhury's UKRI Future Leader Fellowship [MR/T020423/1].

References

Bogacz, R., Brown, E., Moehlis, J., Holmes, P., Cohen, J.D., 2006. The physics of optimal decision making: A formal analysis of models of performance in two-alternative forced-choice tasks. Psychological Review 113, 700–765. doi:10.1037/0033-295X.113.4.700.

Camara, F., Bellotto, N., Cosar, S., Weber, F., Nathanael, D., Althoff, M., Wu, J., Ruenz, J., Dietrich, A., Markkula, G., Schieben, A., Tango, F., Merat, N., Fox, C., 2021. Pedestrian models for autonomous driving part ii: High-level models of human behavior. IEEE Transactions on Intelligent Transportation Systems 22, 5453–5472. doi:10.1109/TITS.2020.3006767.

Ghaderi-Kanghavari, A., Rad, J.A., Nunez, M.D., 2023. A general integrative neurocognitive modeling framework to jointly describe EEG and decision-making on single trials. Computational Brain & Behavior 6, 317–376. doi:10.1007/s42113-023-00167-4.

Kelly, S.P., O'Connell, R.G., 2013. Internal and external influences on the rate of sensory evidence accumulation in the human brain. The Journal of Neuroscience 33, 19434–19441. doi:10.1523/JNEUROSCI.3355-13.2013.

Lin, Y.S., Srinivasan, A.R., Leonetti, M., Billington, J., Markkula, G., 2022. A utility maximization model of pedestrian and driver interactions. IEEE Access 10, 118888–118899. doi:10.1109/ACCESS.2022.3213363.

Ma, S., Yan, X., Billington, J., Leonetti, M., Merat, N., Markkula, G., 2025. Improving models of pedestrian crossing behavior using neural signatures of decision-making. Transportation Research Part F: Traffic Psychology and Behaviour 109, 1491–1506. doi:10.1016/j.trf.2025.01.047.

Malhotra, G., Leslie, D.S., Ludwig, C.J.H., Bogacz, R., 2018. Time-varying decision boundaries: insights from optimality analysis. Psychonomic Bulletin & Review 25, 971–996. doi:10.3758/s13423-017-1340-6.

Markkula, G., Lin, Y.S., Srinivasan, A.R., Billington, J., Leonetti, M., Kalantari, A.H., Yang, Y., Lee, Y.M., Madigan, R., Merat, N., 2023. Explaining human interactions on the road by large-scale integration of computational psychological theory. PNAS Nexus 2, pgad163. doi:10.1093/pnasnexus/pgad163.

Markkula, G., Madigan, R., Nathanael, D., Portouli, E., Lee, Y.M., Dietrich, A., Billington, J., Schieben, A., Merat, N., 2020. Defining interactions: a conceptual framework for understanding interactive behaviour in human and automated road traffic. Theoretical Issues in Ergonomics Science 21, 728–752. doi:10.1080/1463922X.2020.1736686.

Nunez, M.D., Vandekerckhove, J., Srinivasan, R., 2017. How attention influences perceptual decision making: Single-trial EEG correlates of drift-diffusion model parameters. Journal of Mathematical Psychology 76, 117–130. doi:10.1016/j.jmp.2016.03.003.

O'Connell, R.G., Dockree, P.M., Kelly, S.P., 2012. A supramodal accumulation-to-bound signal that determines perceptual decisions in humans. Nature Neuroscience 15, 1729–1735. doi:10.1038/nn.3248.

Palestro, J.J., Bahg, G., Sederberg, P.B., Lu, Z.L., Steyvers, M., Turner, B.M., 2018. A tutorial on joint models of neural and behavioral measures of cognition. Journal of Mathematical Psychology 84, 20–48. doi:10.1016/j.jmp.2018.03.003.

Pekkanen, J., Giles, O.T., Lee, Y.M., Madigan, R., Daimon, T., Merat, N., Markkula, G., 2022. Variable-drift diffusion models of pedestrian road-crossing decisions. Computational Brain & Behavior 5, 60–80. doi:10.1007/s42113-021-00116-z.

Purcell, B.A., Heitz, R.P., Cohen, J.Y., Schall, J.D., Logan, G.D., Palmeri, T.J., 2010. Neurally constrained modeling of perceptual decision making. Psychological Review 117, 1113–1143. doi:10.1037/a0020311.

Radev, S.T., Schmitt, M., Schumacher, L., Elsemüller, L., Pratz, V., Schälte, Y., Köthe, U., Bürkner, P.C., 2023. Bayesflow: Amortized bayesian workflows with neural networks. Journal of Open Source Software 8, 5702. doi:10.21105/joss.05702.

Ratcliff, R., 1978. A theory of memory retrieval. Psychological Review 85, 59–108.

Ratcliff, R., McKoon, G., 2008. The diffusion decision model: Theory and data for two-choice decision tasks. Neural Computation 20, 873–922. doi:10.1162/neco.2008.12-06-420.

Turner, B.M., Forstmann, B.U., Wagenmakers, E.J., Brown, S.D., Sederberg, P.B., Steyvers, M., 2013. A bayesian framework for simultaneously modeling neural and behavioral data. NeuroImage 72, 193–206. doi:10.1016/j.neuroimage.2013.01.048.

Turner, B.M., van Maanen, L., Forstmann, B.U., 2015. Informing cognitive abstractions through neuroimaging: The neural drift diffusion model. Psychological Review 122, 312–336. doi:10.1037/a0038894.

van Vugt, M.K., Beulen, M.A., Taatgen, N.A., 2019. Relation between centro-parietal positivity and diffusion model parameters in both perceptual and memory-based decision making. Brain Research 1715, 1–12. doi:10.1016/j.brainres.2019.03.008.

Yau, Y., Hinault, T., Taylor, M., Cisek, P., Fellows, L.K., Dagher, A., 2021. Evidence and urgency related EEG signals during dynamic decision-making in humans. The Journal of Neuroscience 41, 5711–5722. doi:10.1523/JNEUROSCI.2551-20.2021.